The autophagy protein, ATG14 safeguards against unscheduled pyroptosis activation to enable embryo transport during early pregnancy

Pooja Popli[1], Arin K. Oestreich[2,3], Vineet K. Maurya[4], Marina N. Rowen[2,3], Ramya Masand[1], Michael J. Holtzman[5], Yong Zhang[5], John Lydon[4], Shizuo Akira[6,7], Kelle H. Moley[2,3], and Ramakrishna Kommagani[1,8*]

[1]Department of Pathology and Immunology, Baylor College of Medicine, One Baylor Plaza, Houston, TX 77030, USA

[2]Department Obstetrics and Gynecology,
[3]Center for Reproductive Health Sciences, Washington University School of Medicine, St. Louis, MO, 63110, USA

[4]Department of Molecular and Cellular Biology, Baylor College of Medicine, One Baylor Plaza, Houston, TX 77030, USA

[5]Department of Medicine and Department of Cell Biology, Washington University School of Medicine, St. Louis, MO, 63110, USA

[6]Department of Host Defense, Research Institute for Microbial Diseases (RIMD),
[7]Laboratory of Host Defense, World Premier Institute Immunology Frontier Research Center (WPI-IFReC), Osaka University, Osaka 565-0871, Japan

[8]Department of Molecular Virology and Microbiology, Baylor College of Medicine, One Baylor Plaza, Houston, TX 77030, USA

***Correspondence to:**

Ramakrishna Kommagani
Associate Professor
Department of Pathology and Immunology
Department of Molecular Virology and Microbiology
Alkek Center for Metagenomics and Microbiome Research
T228A, One Baylor Plaza
Baylor College of Medicine
Houston, TX, 77030
Email: Rama.Kommagani@bcm.edu
Phone: (713)-798-5085
Fax: 713-798-5838

Short title: Self-digestion for female reproductive tract functions

The authors have declared that no conflict of interest exists.

Non-standard Abbreviations

WT: Wild Type

HESCs: Human Endometrial stromal cells

dpc: Days post coitum

E2: Estrogen

P4: Progesterone

cKO: conditional knockout

Keywords: Early pregnancy loss, autophagy, fallopian tube, embryo transport, and inflammation

Abstract

Recurrent pregnancy loss (RPL), characterized by two or more failed clinical pregnancies, poses a significant challenge to reproductive health. In addition to embryo quality and endometrial function, proper oviduct function is also essential for successful pregnancy establishment. Therefore, structural abnormalities or inflammation resulting from infection in the oviduct may impede the transport of embryos to the endometrium, thereby increasing the risk of miscarriage. However, the precise cellular mechanisms that maintain the structural and functional integrity of the oviduct are not studied yet. Here, we report that autophagy is critical for maintaining the oviduct homeostasis and keeping the inflammation under check to enable embryo transport. Specifically, the loss of the autophagy-related gene, *Atg14* in the oviduct causes severe structural abnormalities compromising its cellular plasticity and integrity leading to the retention of embryos. Interestingly, the selective loss of *Atg14* in oviduct ciliary epithelial cells did not impact female fertility, highlighting the specificity of ATG14 function in distinct cell types within the oviduct. Mechanistically, loss of *Atg14* triggered unscheduled pyroptosis leading to inappropriate embryo retention and impeded embryo transport in the oviduct. Finally, pharmacological activation of pyroptosis in pregnant mice led to an impairment in embryo transport. Together, we found that ATG14 safeguards against unscheduled pyroptosis activation to enable embryo transport from the oviduct to uterus for the successful implantation. Of clinical significance, these findings provide possible insights on the underlying mechanism(s) of early pregnancy loss and might aid in developing novel prevention strategies using autophagy modulators.

Introduction

A successful pregnancy is orchestrated by the sequential and coordinated events happening in the FRT [1]. Each of these events is crucial to advance to the next step in pregnancy. For example, as a first step, the ovary undergoes ovulation to release a mature ovum into the oviduct where it gets fertilized by the sperm, and a zygote is formed in the ampullary region of the oviduct. The newly formed zygote undergoes several rounds of cleavage to form a morula while being transported through the isthmus region of the oviduct. Timely transport of the embryos from the oviduct into the uterus and synchronous development of the implantation-competent blastocyst and a receptive uterus is a prerequisite for implantation initiation [2]. Any perturbations in these early pregnancy events can lead to adverse ripple effects that can compromise pregnancy outcomes. Previous studies have reported that impaired oviductal transport of embryos can lead to pregnancy failure and cause infertility in mice [3-6]. However, the underlying mechanism is not yet completely understood.

Autophagy is a cellular process, evolutionarily conserved from yeast to mammals, that recycles long-lived proteins and organelles to maintain cell energy homeostasis. Autophagy is classically activated through the nutrient sensor or mammalian target of the rapamycin complex. Genetic screens for autophagy-defective mutants in yeast and other fungi have currently identified 41 autophagy-related (ATG) genes that play a primary role in autophagy [7, 8]. Approximately half of these genes have homologs in higher organisms, and *Atg14* (also known as Barkor for Beclin 1 (*Becn1*)-associated autophagy-related key regulator) is one of them [9, 10]. ATG14 is part of a protein complex that is composed of Beclin 1, vacuolar sorting protein 15 (VPS15), and VPS34 (also named as Pik3c3, the catalytic subunit of the class III phosphatidylinositol 3-kinase), and this ATG14-containing complex plays an important role in the initiation process of autophagy.

With a better understanding of the fundamental process of autophagy, its pathophysiological functions have begun to be appreciated in the female reproductive tract.

For example, mice deficient in key autophagy genes such as genetic knockout of *Atg7* or *Becn1* result in primary ovarian insufficiency and reduced progesterone production [11, 12]. Similarly, recent studies from our group established the roles of three different autophagy-specific genes: ATG16L, FIP200/RB1CC1, or BECN1 in endometrial physiological processes, including receptivity and decidualization [13-15]. However, none of these proteins exhibited any discernible impact on oviduct function. Surprisingly, in this study, we revealed a critical role for Atg14 in maintaining proper oviduct function, specifically enabling the transport of embryos to the uterus—a function distinct from that of other autophagy-related proteins. Loss of Atg14 in the oviduct resulted in severe structural abnormalities, compromising its cellular plasticity and integrity, ultimately leading to embryo retention and infertility.

Materials and Methods

Animal care and use:

All animal studies were approved by the Institutional Animal Care and Use Committee of Washington University School of Medicine, Saint Louis, MO, USA and Use Committee of Baylor College of Medicine, Houston, TX, USA. *Atg14* f/f mice were provided by gift from Dr. Shizuo Akira at the Department of Host Defense, Research Institute for Microbial Diseases (RIMD), Osaka University, and previously described [16]. Wild type Pr-cre mice were provided by Dr. John Lydon at Baylor College of Medicine, Houston and previously described [17]. Atg14$^{flox/flox}$ mice, in which exon 4 was flanked by loxp sites, were bred to progesterone receptor cre (PR$^{cre/+}$) mice to generate (Atg14$^{flox/flox}$; PR$^{cre/+}$ mice), hereafter referred to as *Atg14* cKO mice. Both control and conditional knockout females were generated by crossing females carrying homozygous *Atg14*$^{flox/flox}$ alleles with *Atg14* cKO males. *Foxj1-cre* mice were a generous gift from Dr. Michael J. Holtzman at Washington University St. Louis and previously described [18]. *Foxj1*/*Atg14* cKO mice were generated by crossing females carrying homozygous *Atg14* $^{f/f}$/Foxj1$^{f/f}$ females with *Atg14*$^{f/f}$/*Foxj1-cre* males. All mice were age-matched and on a C57BL/6 genetic background (The Jackson Laboratory, Bar Harbor, ME). Mice were genotyped by PCR analysis of genomic DNA isolated from tail clippings using the gene-specific primers listed in **Supplementary Table 1.**

Fertility analysis and timed mating

Female fertility was determined by mating cohorts of *Atg14* cKO experimental (n=6) and control *Atg14* f/f (n=4) females individually starting at 8 weeks of age with sexually mature males of proven fertility. Similarly, breeding trials were set up for *Foxj1/Atg14*-cre females (n=6) and *Foxj1*/*Atg14* control 8-week-old f/f females (n=6). The numbers of litters and pups were tracked over 6 months for each female. Pups per litter for each genotype are reported as mean ± SEM. For timed mating, the morning on which the copulatory plug was first observed was considered 1 dpc. To visualize implantation sites, mice received a tail vein

injection of 50 µL of 1% Chicago Sky Blue dye (Sigma-Aldrich, St. Louis, MO, USA) at 5 dpc just before sacrifice.

Steroid hormone treatments

The hormonal profile of pregnancy at the time of implantation was done using a previously described experimental scheme [14]. Briefly, *Atg14* cKO and control females (8 weeks old) were bilaterally ovariectomized under ketamine anesthesia with buprenorphine-SR as an analgesic. Mice were allowed to rest for two weeks to dissipate all endogenous ovarian hormones. After the resting period, mice were injected with 100 ng of estrogen (E2; Sigma-Aldrich) dissolved in 100 µL of sesame oil on two consecutive days and then allowed to rest for two days. At this point, mice were randomly divided into three groups of five: Vehicle-treated (E2 priming) mice received four consecutive days of sesame oil injections; E2 group mice received three days of sesame oil injections followed by a single injection of 50 ng of E2 on the fourth day; The E2/P4 mice received 1 mg of progesterone (P4; Sigma-Aldrich) for three consecutive days followed by a single injection of 1 mg P4 plus 50 ng E2 on the fourth day. All hormones were delivered by subcutaneous injection in a 90:10 ratio of sesame oil: ethanol. Mice were euthanized 16 hours after the final hormone injection to collect the uteri. A small piece of tissue from one uterine horn was processed in 4% neutral buffered paraformaldehyde for histology, and the remaining tissue was snap-frozen and stored at -80 °C.

Hematoxylin and eosin staining

Tissues were fixed in 4% paraformaldehyde, embedded in paraffin, and then sectioned (5 µm) with a microtome (Leica Biosystem, Wetzlar, Germany). Tissue sections were deparaffinized, rehydrated, and stained with Hematoxylin and Eosin (H&E) as described previously [19]. All the histology was performed on three sections from each tissue of individual mice, and one representative section image is shown in the respective figures.

Histological analysis

For histological analysis, the collected tissues (oviduct or uteri) were fixed in 4% paraformaldehyde, embedded in paraffin, and sectioned. Sections (5 µm) were immunostained (n=5 per group) as described previously [19]. Briefly, after deparaffinization, sections were rehydrated in an ethanol gradient and then boiled for 20 min. in citrate buffer (Vector Laboratories Inc., Newark, CA, USA) for antigen retrieval. Endogenous peroxidase activity was quenched with Bloxall (Vector Laboratories Inc.), and tissues were blocked with 2.5% goat serum in PBS for 1 hr (Vector Laboratories Inc.). After washing in PBS three times, tissue sections were incubated overnight at 4 °C in 2.5% goat serum containing the primary antibodies listed in **Supplementary Table 2.** Sections were incubated for 1 hr with biotinylated secondary antibody, washed, and incubated for 45 min with ABC reagent (Vector Laboratories Inc.). Color was developed with 3, 3'-diaminobenzidine (DAB) peroxidase substrate (Vector Laboratories Inc.), and sections were counter-stained with hematoxylin. Finally, sections were dehydrated and mounted in Permount histological mounting medium (Thermo Fisher Scientific, Waltham, MA, USA).

Transmission electron microscopy (TEM)

For ultrastructural analysis, oviducts were fixed in 2% paraformaldehyde/2.5% glutaraldehyde (Ted Pella Inc., Redding, CA) in 100 mM cacodylate buffer, pH 7.2 for 1 hr at room temperature and then overnight at 4°C. Samples were washed in cacodylate buffer and postfixed in 1% osmium tetroxide (Ted Pella Inc.) for 1 hr. Samples were then rinsed extensively in dH20 prior to en bloc staining with 1% aqueous uranyl acetate (Ted Pella Inc.) for 1 hr. Following several rinses in dH20, samples were dehydrated in a graded series of ethanol and embedded in Eponate 12 resin (Ted Pella Inc.). For initial evaluation semithin sections (0.5 µm) were cut with a Leica Ultracut UCT7 ultramicrotome (Leica Microsystems Inc., Bannockburn, IL) and stained with toluidine blue. Sections of 95 nm were then cut and stained with uranyl acetate and lead citrate and viewed on a JEOL 1200 EX II transmission electron microscope (JEOL USA Inc., Peabody, MA). Images at magnifications of 3,000X to

30,000X were taken with an AMT 8-megapixel digital camera (Advanced Microscopy Techniques, Woburn, MA).

Immunofluorescence analysis

Formalin-fixed and paraffin-embedded sections were deparaffinized in xylene, rehydrated in an ethanol gradient, and boiled in a citrate buffer (Vector Laboratories Inc.) for antigen retrieval. After blocking with 2.5% goat serum in PBS (Vector laboratories) for 1 hr at room temperature, sections were incubated overnight at 4°C with primary antibodies (**Supplementary Table 2**) diluted in 2.5% normal goat serum. After washing with PBS, sections were incubated with Alexa Fluor 488-conjugated secondary antibodies (Life Technologies, Carlsbad, CA, USA) for 1 hr at room temperature, washed, and mounted with ProLong Gold Antifade Mountant with DAPI (Thermo Fisher Scientific). All Immunofluorescence images were obtained using a Zeiss LSM 880 confocal microscope (10x and 40x objective lens).

Western blotting

Protein lysates (40 µg per lane) from uteri or oviducts were loaded on a 4-15% SDS-PAGE gel (Bio-Rad, Hercules, CA, USA), separated in 1X Tris-Glycine Buffer (Bio-Rad), and transferred to PVDF membranes via a wet electro-blotting system (Bio-Rad), all according to the manufacturer's directions [20]. PVDF membranes were blocked for 1 hour in 5% non-fat milk in Tris-buffered saline containing 0.1% Tween-20 (TBS-T, Bio-Rad), then incubated overnight at 4 °C with antibodies listed in **Supplementary Table 2** in 5% BSA in TBS-T. Blots were then probed with anti-Rabbit IgG conjugated with horseradish peroxidase (1:5000, Cell Signaling Technology, Danvers, MA, USA) in 5% BSA in TBS-T for 1 hr at room temperature. Signal was detected with the Pierce™ ECL Western Blotting Substrate (Millipore, Billerica, MA, USA), and blot images were collected with a Bio-Rad ChemiDoc imaging system.

RNA Isolation and Quantitative Real-Time RT-PCR Analysis

Tissues/cells were lysed in RNA lysis buffer, and total RNA was extracted with the Purelink RNA mini kit (Invitrogen, Carlsbad, CA, USA) according to the manufacturer's instructions. RNA was quantified with a Nano-Drop 2000 (Thermo Fisher Scientific). Then, 1 µg of RNA was reverse transcribed with the High-Capacity cDNA Reverse Transcription Kit (Thermo Fisher Scientific). The amplified cDNA was diluted to 10 ng/µL, and qRT-PCR was performed with primers listed in the **Supplementary Table 1** and TaqMan 2X master mix (Applied Biosystems/Life Technologies, Grand Island, NY, USA) on a 7500 Fast Real-time PCR system (Applied Biosystems/Life Technologies). The delta-delta cycle threshold method was used to normalize expression to the reference gene 18S.

Treatment of mice with Polyphyllin VI

Polyphyllin VI (Selleck chemicals, Houston, TX, USA), a pharmacological agent that induces caspase-1-mediated pyroptosis, was used to study its effects on embryo transport in the oviduct [21]. Eight-week-old C57BL/6 mice were injected for three consecutive days starting from 1 dpc with Polyphyllin VI activator dissolved in 40% PEG-300 (15mg/kg body weight)**.** Dimethyl sulfoxide with 40% PEG-300 was administered as a vehicle.

Transfection and human endometrial stromal cell (HESC) decidualization

HESCs were plated in six-well culture plates at a cell density of $1x10^5$ per well in triplicates. For siRNA-mediated knockdown of *Atg14*, HESCs were treated with Lipofectamine RNAiMAX reagent (Thermo Fisher Scientific, Waltham, MA)) and 60 pmol of either non-targeting siRNA (D-001810-10-05) or siRNAs targeting *Atg14* (L-020438-01-0005). Six hours after the transfection, the media was replaced with complete HESC media. 48 hrs later, HESCs were treated with Opti-MEM (Thermo Fisher Scientific) reduced serum media containing 2% fetal bovine serum (FBS), E2 (100 nM), 10 mM medroxyprogesterone acetate (MPA, Sigma-Aldrich) and 50 mM cAMP (Sigma-Aldrich), which constitutes the decidualization media. The first day that HESCs were cultured in decidualization media was assigned day 0. Decidualization media was renewed every two days. Cells were harvested at appropriate time points as per experimental conditions. Total RNA was isolated to assess

transcript levels of the decidualization markers: prolactin (PRL) and insulin-like growth factor binding protein-1 (IGFBP-1).

Statistics

A two-tailed paired student t-test was used to analyze data from experiments with two experimental groups and one-way ANOVA followed by Tukey's post hoc multiple range test was used for multiple comparisons. All data are presented as mean ±SEM. GraphPad Prism 9 software was used for all statistical analyses. Statistical tests, including p values, are reported in the corresponding figure legends or, when possible, directly on the data image. To ensure the reproducibility of our findings, experiments were replicated in a minimum of three independent samples, to demonstrate biological significance, and at least three independent times to ensure technical and experimental rigor and reproducibility.

Results

Conditional deletion of *Atg14* in the FRT results in infertility despite the normal ovarian function

To explore the role of *Atg14* in uterine function, we first determined its expression levels in uterus during early pregnancy (Day 1-7) in mice. We found distinct expression of ATG14 in all the uterine compartments (luminal epithelium, glands, and stroma) by day 1 of pregnancy, which disappeared by day 2 of pregnancy (**Fig. 1A**). However, the ATG14 expression in uterus reappeared by day 3 and persisted through the day 7 of pregnancy. The period from day 3 to day 7 is critical, as it is during this time when uterus begins to prepare for embryo implantation and undergoes decidualization process. Consistent with protein expression, similar *Atg14* expression at mRNA levels was noted in uteri from early pregnant mice (**Fig. 1B**). This analysis suggests a potential role for ATG14 protein in the uterine physiologic adaptations during early pregnancy. Thus, to study the role of ATG14 in uterine function, we generated a conditional knockout ($PR^{cre/+}$ /$Atg14^{flox/flox}$) mouse model by crossing *Atg14* flox/flox mice with mice expressing Cre recombinase under the control of progesterone receptor promoter ($PR^{cre/+}$). Histological examination of the uterus from adult females showed no gross morphological differences between *Atg14* cKO and control mice (**Fig. S1A**). Further, we did not find any overt defects in ovary as cKO mice had normal follicles and corpus luteum as like their corresponding controls (**Fig. S1B**). Analysis of transcript levels from the uterus, ovary, and liver showed that while *Atg14* levels were efficiently depleted in uteri from cKO mice the levels were unaltered in the ovary and liver samples in control and cKO mice (**Fig. 1C**). Immunofluorescence analysis further confirmed the efficient deletion of ATG14 in all uterine compartments (epithelium and stroma) of cKO mice uteri compared to corresponding control groups (**Fig. 1D**).

Considering the effective ablation, a 6-month breeding study was performed mating virile wild-type male mice with adult *Atg14* cKO and control female mice. We found that *Atg14* cKO females did not deliver any litter during 6-months trial period. However, the control female (*Atg14* flox/flox) mice delivered an average of ~7-8 pups per litter every

month (**Table 1**) (**Fig. 1E & F.** These findings suggest an indispensable role of *Atg14* in female fertility with intact ovarian function.

Loss of *Atg14* results in impaired embryo implantation and uterine receptivity in mice

Based on the normal ovarian morphology, we posited that the infertility observed in females with *Atg14* cKO status could be attributed to compromised uterine functioning. Analysis of the implanting embryos at Day 5 of pregnancy found no implantation sites in the uteri of *Atg14* cKO females, whereas ~8 to 9 implantation sites were seen in the uteri of control mice at 5 dpc (**Fig. 2A, left panel**). Whilst there was no embryo present in the uterine lumen of *Atg14* cKO mice, a fully attached embryo encapsulated by the luminal uterine epithelium, were seen in control mice uteri were (**Fig. 2A, middle panel**). Additionally, MUC1, a receptive marker expression was persisted in the luminal epithelium of cKO mice uteri at 5 dpc as well as 4 dpc (**Fig. 2A, right panel, Fig. S2A**). The process of successful embryo attachment and implantation within the uterus necessitates a transition from a non-receptive to a receptive state, a transformation orchestrated under the regulated influence of steroid hormones. Thus, the effects of *Atg14* loss on uterine responsiveness to steroid hormones E2 and P4 was characterised. We performed an established hormone-induced uterine receptivity experiment, which involved ordered and co-stimulatory actions of E2 and P4 leading to the initiation of a receptive phase [22]. In response to E2 treatment, uteri from both *Atg14* control and cKO mice showed similar proliferation as evidenced from Ki-67 staining (**Fig. 2B, middle panel**). Following the co-stimulation with E2+P4 treatment, epithelial proliferation was inhibited with concomitant induction of stromal cell proliferation in control mice uteri indicating fully receptive uteri (**Fig. 2C**). Interestingly, cKO mice uteri failed to elicit sub-epithelial stromal cell proliferation and showed intact P4-driven inhibition of epithelial proliferation. Consistently, uteri from *Atg14* cKO mice at 4 dpc showed reduced number of proliferating stromal cells (**Fig. S2B**). These results demonstrate that ATG14 is required for P4-mediated but not for E2-mediated actions during uterine receptivity.

Given that stromal cell proliferation is a prerequisite for successful decidualization, we wondered whether cKO mice uteri can undergo the decidualization process. The uteri of *Atg14* cKO mice failed to respond to oil injection and did not show any increase in size, reflecting their failure to undergo decidualization. (**Fig. 2C, left panel**). Further, a significant reduction in proliferative pH3-positive and multinucleated decidualized stromal cells were noted in cKO mice stimulated uterine horns (**Fig. 2C**). Also, the decidualization markers *Wnt4* and *Bmp2* was significantly reduced in stimulated horns of cKO mice compared to control mice (**Fig. 2D)**. We determined next whether ATG14 is likewise required for HESCs decidualization. Control siRNA transfected cells when treated with EPC seemed to change their morphological transformation from fibroblastic to epithelioid (**Fig. 2E**) and had increased expression of the decidualization markers *IGFBP1* and *PRL* by day three only (**Fig. 2F**). In contrast, HESCs with *ATG14* knockdown failed to undergo morphological transformation with concomitant reduction in *PRL* and *IGFBP1* marker expression (**Fig. 2F**). Together, these results underscore the critical role of ATG14 in embryo implantation, uterine receptivity, and the decidualization.

***Atg14* is required for maintaining oviductal cell plasticity and embryo transport**

Given that *Atg14* cKO mice had impaired embryo implantation, we wondered whether embryos are reaching the uterus timely through oviduct. To determine this, we flushed embryos from both the control and cKO mice uteri on day 4 of pregnancy. Interestingly, in cKO mice, we could retrieve only 1-2% of embryos from their uteri, whereas in control mice, 100% of well-developed blastocysts were retrieved from their uteri (**Fig. 3A, Upper and lower panel**). To ensure the timely transport of all embryos from the oviducts to the uteri, we also flushed oviducts from both control and cKO mice. As expected, in the control mice oviduct flushing, we could not recover any embryos or blastocysts, indicating their precise and timely transport to the uterus. Unexpectedly, oviduct flushing from cKO mice resulted in the retrieval of approximately 80-90% of blastocysts, suggesting their potential entrapment within the oviducts, impeding their transit to the uterus (**Fig. 3B**). Similarly, when we super-

ovulated the mice and looked for the embryos on the day 4 of pregnancy, we could recover ~20-25 embryos from the cKO mice oviducts compared to only 4-5 embryos that were able to reach the uterus. In comparison, in control mice, 90% of embryos were able to complete their pre-destined and timely transport to the uterus (**Fig. 3C**), except 1-2% of unfertilized embryos, which remained in their oviducts.

To understand the underlying cause for retained embryos in cKO mice oviducts, we performed histology analysis and determined the structural morphology of their oviducts. The cKO mice oviduct lining shows marked eosinophilic cytoplasmic change akin to decidualization in human oviducts. Some of the cells showed degenerative changes with cytoplasmic vacuolization and nuclear pyknosis, loss of nuclear polarity, and loss of distinct cell borders giving an appearance of fusion of cells (**Fig. 3D**). The marked cytologic enlargement appears to cause luminal obliteration or narrowing resulting in a completely unorganized, obstructed, and narrow lumen, thereby, hampering the path of embryos to reach the uterus as evident from an entrapped embryo shown in **Fig. 3B**. Further, epithelial (cytokeratin KRT8-positive) and myosalpinx (α-smooth muscle active [SMA]-positive,) marker analysis revealed completely distorted epithelial structures (in terms of loss of epithelial cell integrity or plasticity). However, there were no overt defects in the muscle organization in oviducts of cKO mice (**Fig. 3D**). To gain more insights into structural defects, we performed TEM analysis on oviducts collected from both control and cKO females on day 4 of pregnancy. Interestingly, oviducts from cKO females had numerous altered mitochondrial structures with abnormally enlarged mitochondria and a less dense matrix compared to control oviducts that had small and compact mitochondria with tight cristae and a dense matrix (**Fig. 3E**). Together, these results demonstrate that Atg14 is required for maintaining oviductal cell plasticity and embryo transport.

Selective loss of *Atg14* in oviduct cilia is dispensable for female fertility

The oviduct epithelium primarily consists of two types of cells: ciliated and secretory (non-ciliated) cells. Ciliated cells play a role in embryo and oocyte transport by means of

ciliary beat, and non-ciliated/secretory cells produce an oviductal fluid that is rich in amino acids and various molecules, thereby providing an optimal micro-environment for sperm capacitation, fertilization, embryonic survival, and development [23]. Therefore, we determined whether oviducts from cKO mice possess normal ciliated and secretory cell composition. To do so, we examined the expression of various markers, including acetylated-α-tubulin (cilia marker), FOXJ1 (ciliogenesis markers), and PAX8 (non-ciliated/ secretory cell marker). As shown in **Fig. 4A,** while we observed normal ciliary structures in the ampulla of both control and cKO oviducts, there was a remarkable reduction in the ciliary cells (indicated by fewer α-tubulin and FOXJ1-positive cells) as well as secretory cells (indicated by fewer PAX-8 positive cells) in the isthmus of cKO oviducts (**Fig. 4A & B)**.

Given the importance of cilia in embryo transport, we wondered whether the loss of *Atg14* in oviduct cilia has any impact on embryo transport. To address this, we generated a *Foxj1*-cre/+; *Atg14* f/f mouse model, wherein *Atg14* will be ablated only in ciliary epithelial cells. Interestingly, the 6-month breeding trial revealed that loss of *Atg14* in oviductal cilia had no impact on fertility (**Table 2**, **Fig. 4C & D**). Consistently, D5 implantation study analysis showed ~7-8 visible embryo implantation sites in *Foxj1/Atg14* cKO mice like their corresponding controls suggesting that embryos were able to make their way to the uterus in a timely manner and undergo implantation despite the ablation of *Atg14* in the oviduct ciliary epithelial cells (**Fig. 4E**). These findings suggest that ciliary expression of *Atg14* is dispensable for embryo transport.

Atg14 **prevents unscheduled pyroptosis activation in the oviduct to enable embryo transport**

Having identified the cellular mechanisms of Atg14, we aimed to delineate the underlying molecular mechanisms associated with Atg14 function in oviduct. Since, we found mitochondrial defects with ATG14 loss and altered mitochondrial structures have been linked to the activation of pyroptosis, we determined if ATG14 regulates pyroptosis in oviduct [24-26]. First, we assessed the key primary executors of the pyroptosis pathway, GSDMD

and caspase-1. Immunofluorescence analysis revealed a remarkable upregulation in GSDMD and caspase-1 expression in the cKO oviducts compared to controls (**Fig. 5A & B**). Consistently, western blot analysis also confirmed elevated expression of caspase-1 and GSDMD in cKO oviducts in comparison to control oviducts as shown in **Fig. 5C.** The qPCR analysis further demonstrated elevated levels of inflammatory markers, such as *Tnf-α* and *Cxcr3* in cKO oviducts compared to control ones (**Fig. 5D**). Based on these findings, we posit that Atg14 exerts a regulatory control over the pyroptotic pathway and activation of pyroptosis owing to loss of ATG14 within the oviduct adversely impacts embryo transport. However, to substantiate the aforementioned notion, we also evaluated the impact of unscheduled activation of pyroptosis on the embryo transport. To test this, we employed a pyroptosis inducer, Polyphyllin VI and chose the optimal dose based on the established studies [21]. Wild type females were mated with virile males and following the plug detection treated with Polyphyllin VI for three consecutive days from 1 to 4 dpc (**Fig. 5E**). We chose to treat to 1 to 4 dpc for treatment to activate unwarranted pyroptosis in oviduct prior to embryo transport. Following the treatments, the oviducts, and uteri from both vehicle-treated and Polyphyllin VI-treated were flushed. We found that pregnant females treated with Polyphyllin VI showed ~50% embryo retention in the oviduct, whereas in the vehicle-treated group, no embryos were retained in the oviduct (**Fig. 5F & G**). Precisely activating the unscheduled pyroptosis during the critical period of embryo transport is technically challenging. Nonetheless, our findings provide evidence that unscheduled pyroptosis adversely affects embryo transport through the oviduct. Taken together, these results demonstrate that *Atg14* safeguards pyroptosis activation in the oviduct and allows the smooth transport of embryos to the uterus (**Fig. 5H**).

Discussion

In this study, we delineated the essential role of ATG14 in maintaining the structural integrity of the oviduct by preventing pyroptosis, which enables smooth embryo transit during early pregnancy. Specifically, we dissected the tissue-specific functions of ATG14 in the FRT using Cre driver mice targeting female reproductive tract. Given that PR-Cre expresses postnatally in different tissues of FRT such as corpus luteum, oviducts, and different cellular compartments (epithelial, stromal, and myometrium) of uteri [17], we found that conditional ablation of ATG14-mediated functions in FRT resulted in infertility owing to hampered transport of embryos from the oviduct. Additionally, *Atg14* loss in uteri causes impaired embryo implantation, receptivity, and decidualization. Its ablation in the oviduct causes activation of pyroptosis, an inflammatory-associated apoptosis pathway that causes the retention of embryos in the oviduct and prevents their timely transport to the uterus. However, the ovarian-specific functions were found to be unaffected despite the loss of *Atg14* in the corpus luteum.

The human endometrium is a complex dynamic tissue that undergoes sequential phases of proliferation and differentiation to support embryo implantation during the conceptive. However, in absence of implanting embryo, endometrium sheds (menstruation) and initiates regeneration process [27]. Previous reports indicated that autophagy is modulated in the human endometrium during the menstrual cycle. For example, autophagy altered during the proliferative and secretory phases of the menstrual cycle with its highest activity occurring during the secretory phase when the stroma is decidualized [28]. Similarly, the level of autophagy was higher in postmenopausal human uterine epithelial cells compared to premenopausal uterine epithelial cells indicating the onset of autophagy upon estrogen deprivation [29]. Although all these studies reported that autophagy is hormonally regulated, however, the role of autophagy-specific proteins in the endometrium is not established till our group's recent reports. Specifically, studies from our group reported the role of three different autophagy-associated proteins: FIP200 [13], ATG16L [15], and BECLIN-1 in uterine functions [14]. Conditional ablation of *Fip200* and *Atg16l* in the uterus

displayed fertility defects owing to impaired implantation, uterine receptivity, and decidualization defects. On contrary, loss of *Beclin1* in the uterus caused progressive loss of endometrial progenitor stem cells resulting in severe uterine developmental defects and rendered the mice infertile [14]. Although the autophagy-related proteins we studied so far influenced uterine functions, [13-15], we found a distinct role for ATG14 in both the uterine and oviduct-specific functions. It is intriguing to note that the absence of ATG14 did not affect the tissue integrity of the uterus. However, the severe structural abnormalities in the oviduct due to *Atg14* ablation unearthed a unique function of Atg14 in maintaining oviduct homeostasis. This distinctive role of ATG14, unlike other autophagy proteins, might be due to its pivotal role in the assembly of PtdIns3K complexes which is not the case for either FIP200 or ATG16L [27, 30, 31]. Nevertheless, understanding the specific contributions of each core autophagy protein in reproductive tract functions is necessary which requires substantial efforts.

The retention of preimplantation embryos in the oviduct established as a significant contributor to implantation failures, presenting challenges to the overall reproductive health of women [4-6]. Embryo transport in the oviduct is known to be controlled primarily by two major physiological responses: ciliary activity and muscle contractility. In our study, a dramatic decrease in the number of Foxj1^{+ve} ciliary epithelial cells and Pax-8^{+ve} secretory cells in *Atg14* cKO mice implied cell-type specific actions for ATG14 in oviduct. Interestingly, the specific ablation of *Atg14* in Foxj1+ve ciliary epithelial cells of the oviduct does not appear to impact fertility. This suggests that the absence of ATG14 within ciliary cells does not impact the process of embryo transport. Although unexpected, this is consistent with other reports that have demonstrated the dispensability of cilia for embryo transport in the oviduct [4, 5].

Pyroptosis is a highly inflammatory form of programmed cell death, characterized by cell swelling, flattening of the cytoplasm and large bubbles like protrusions on the plasma membrane [32-34]. Several recent studies found a link between autophagy and pyroptosis [35]. *In vivo* studies also found that mice lacking the autophagy genes *Atg14*, *Fip200*, *Atg5*,

or *Atg7* in myeloid cells had more pronounced lung inflammation [36]. In our study, cellular swelling, and fused membranous structures (a unique feature of activation of pyroptosis) observed in the oviductal epithelial folds from *Atg14* cKO mice. This aberrant activation of the pyroptosis pathway due to loss of *Atg14* appear to adversely affect the oviduct cellular plasticity. These findings have implications beyond the oviduct, as autophagy can modulate the inflammatory signalling pathway through different avenues. For example, first, autophagy prevents mitochondrial reactive oxygen species release that can activate the inflammasome by inhibiting IL1-β and IL18 production through the digestion of dysfunctional mitochondria [37]. Second, autophagy is capable of targeting inflammasome complexes for degradation, which prevents the cleavage of pro-IL-1β and pro-IL-18 into biologically active forms. Finally, autophagy machinery further regulates IL-1β levels by engulfing and degrading pro-IL-1β proteins [37]. In our study, accumulation of abnormally enlarged and dysfunctional mitochondria in absence of ATG14 in oviduct clearly suggests induction of severe inflammatory conditions hampering the embryo transit through the oviduct. These findings are further substantiated by the upregulation of pivotal mediators of the pyroptosis program, including GSDMD and caspase-1, in *Atg14* cKO mice. Notably, the induction of pyroptosis in the absence of ATG14 is specifically localized to the oviducts, with no parallel activation detected in either the ovary or uterus. This distinct activation pattern suggests a unique interaction between oviduct-specific proteins and ATG14, which keeps pyroptosis at the bay in the oviduct. Nevertheless, a comprehensive understanding of the oviduct-cell-specific roles of ATG14 necessitates additional investigations, employing oviduct-specific cKO mouse models.

In this report, we revealed tissue-specific roles of ATG14 in governing oviductal transport, and uterine receptivity which are necessary for embryo implantation and pregnancy establishment. Of mechanistic insights, we delineated a novel function of ATG14 as a negative regulator of pyroptosis, which is vital for proper embryo transport in the oviduct (**Fig. 5 H**). Thus, this study not only sheds light on the involvement of autophagy in oviductal embryo transport but also underscores the importance of autophagy in preserving the

oviduct tissue integrity. Such insights hold promise for advancing our understanding of gynaecological pathologies associated with the oviduct including tubal pregnancies.

Acknowledgments

We thank Neil Ghosh, and Goutham Davuluri from our group for the technical assistance. We thank Dr. Robert Lawrence (senior editor at Baylor College of Medicine) for assistance with manuscript editing. We thank WashU Molecular Microbiology Imaging Facility for assisting us with transmission electron microscopy. This work was funded, in part, by the National Institutes of Health/National Institute of Child Health and Human Development (grants R01HD102680, R01HD104813, and R01HD065435) to RK, R01 HD-042311 to JPL, and in part by National Institutes of Health/National Heart, Lung, and Blood Institute (grant R35HL145242) to MJH.

Authors' roles

PP and RK designed experiments, conducted most of the studies, analysed the data, and wrote the manuscript. AKO, VKM and MNR conducted some of the experiments. MJH, JL, SA, YZ, and KHM, provided critical reagents for the study. RM helped us with oviduct pathology phenotype analysis. RK conceived the project, supervised the work, and wrote the manuscript. All authors critically reviewed the manuscript.

Conflict of Interest

The authors have declared that no conflict of interest exists.

Table 1: **Six-month breeding trial of *Atg14* control and cKO females with wild-type males**

Table 2: **Six-month breeding trial of *Foxj1*/*Atg14* control and cKO females with wild-type males**

Figure legends

Figure 1: *Atg14* loss in the FRT results in infertility. (**A**) Representative immunofluorescent images of uteri from pregnant mice at the indicated days of pregnancy stained with an ATG14-specific antibody (green). LE: luminal epithelium, G: glands, S: stroma, Scale bar: 200 µm. (**B**) Relative transcript levels of *Atg14* mRNA in uteri from pregnant mice at indicated days of pregnancy. mRNA levels are normalized to levels of 18S m-RNA. Data are presented as mean ±SEM. (**C**) Relative mRNA levels of *Atg14* in 8-week-old virgin control and cKO mice uteri, ovary, and liver (n=5). mRNA levels are normalized to levels of 18S mRNA. Data are presented as mean ±SEM; ***P<0.001, P>0.05, ns=non-significant. (**D**) Representative immunofluorescent images of ATG14 expression in different uterine compartments in control and *Atg14* cKO mice. (**E**) (*left panel*) Relative number of pups/female and (*right panel*) and relative number of total pups/months of *Atg14* control and cKO mice sacrificed after the breeding trial. Data are presented as mean ±SEM; P>0.05, ns=non-significant.

Figure 2: *Atg14* is critical for embryo implantation, uterine receptivity, and stromal cell decidualization. (**A**) Gross images of 5.0 dpc uteri of control and *Atg14* cKO mice injected with Chicago Sky Blue dye to visualize implantation sites (denoted by black arrows) (*left panel*). H&E-stained cross-sections (4X & 40X) of 5.0 dpc uteri of control and *Atg14* cKO mice to visualize embryo implantation (*Middle panel*). Immunofluorescence analysis of uterine tissues from control and *Atg14* cKO mice, stained with MUC1 and KRT8 (*right panel*). (**B**) Representative immunofluorescence images of uteri from control and *Atg14* cKO mice stained for Ki-67 following Oil or E2 or E2+P4 treatment (n=5 mice/group); scale bar: 100 µm. (**C**) Representative images of uteri (*left*) and uterine histology after artificial decidualization (*middle*). Immunofluorescence analysis of PH3 in decidualized horn of Control and *Atg14* cKO mice. (**D**) Relative transcript levels of *Atg14*, and decidualization markers (*Bmp2* and *Wnt4)* after artificial decidualization. (n=4-6 per group). Data are presented as mean ±SEM. *P < 0.05; **P < 0.01; ***P < 0.001 compared with controls. 18S

was used as an internal control. (**F**) Morphology of human endometrial stromal cells transfected with control or *Atg14* siRNA followed by treatment with decidualization media and (**G**) qPCR analysis of ATG14 and the indicated decidualization markers. Data are presented as mean ±SEM. *P < 0.05; **P < 0.01; ***P < 0.001 compared with controls.

Figure 3: *Atg14* is critical for embryo transport in oviduct. (**A**) Representative images (*upper panel*) and percentage of embryos (*lower panel*) collected at 4 dpc from the uteri or the oviducts of control or *Atg14* cKO mice. (**B**) Histological analysis using H&E staining of the ampullary and isthmic region of the oviduct from control and *Atg14* cKO female mice at 4 dpc (n=3 mice/genotype). (**C**) Embryos retrieved from the oviduct and uterus of super-ovulated *Atg14* control or cKO mice at 4 dpc. (**D**) Immunofluorescence analysis of KRT8 (green), and α-SMA (Red), in oviduct of 4 dpc control and *Atg14* cKO mice. (**E**) TEM of oviducts at 4 dpc from control and *Atg14* cKO.

Figure 4: *Atg14* loss in oviduct cilia is dispensable for embryo transport. (A) Immunofluorescence analysis of acetylated a-tubulin (green), and DAPI (blue) in oviduct of 4 dpc control and *Atg14* cKO mice. (**B**) Immunohistochemical analysis of FOXJ1 and PAX8 at 4 dpc. (**C & D**) Relative number of pups/femalsoyale and relative number of total pups/months of control and *Foxj1*/*Atg14* cKO mice sacrificed after the breeding trial. Data are presented as mean ± SEM; P>0.05, ns=non-significant. (**E**) Gross images of 5.0 dpc uteri of control and *Atg14* cKO mice injected with Chicago Sky Blue dye to visualize implantation sites (denoted by black arrows).

Figure 5: *Atg14* promotes embryo transport in oviduct by preventing pyroptosis activation. Immunofluorescence analysis of GSDMD (red) + KRT8 (green), Caspase-1 (red) + KRT8 (green) in oviducts of adult control and *Atg14* cKO mice. Tissues were counterstained with DAPI (blue) to visualize nuclei; scale bars, 100 µm. (**B**) Immunohistochemical analysis of GSDMD in adult oviduct tissues. (**C**) Western blotting to show protein levels of Caspase-1, and GSDMD in oviduct tissues. β-actin is used as a loading control. (**D**) Relative transcript levels of *Tnf-α* and *Cxcr3* in oviduct tissues. Data are

presented as mean ±SEM. *P<0.05; **P<0.01; ***P<0.001 compared with controls. 18S was used as an internal control. (**E**) Experimental strategy for pyroptosis activation in pregnant female mice. (**F**) Embryos flushed from vehicle or polyphyllin VI treated D-4 pregnant females. (**G**) Percentage of embryos recovered from oviducts or uteri. (**H**) Graphical illustration to show embryo transport and pyroptosis regulation in oviduct.

References

1. Wang, H. and S.K. Dey, *Roadmap to embryo implantation: clues from mouse models.* Nat Rev Genet, 2006. **7**(3): p. 185-99.
2. Croxatto, H.B., *Physiology of gamete and embryo transport through the fallopian tube.* Reprod Biomed Online, 2002. **4**(2): p. 160-9.
3. Jiang, R., et al., *CDC42 governs normal oviduct multiciliogenesis through activating AKT to ensure timely embryo transport.* Cell Death Dis, 2022. **13**(9): p. 757.
4. Herrera, G.G.B., et al., *Oviductal Retention of Embryos in Female Mice Lacking Estrogen Receptor alpha in the Isthmus and the Uterus.* Endocrinology, 2020. **161**(2).
5. Wang, H., et al., *Aberrant cannabinoid signaling impairs oviductal transport of embryos.* Nat Med, 2004. **10**(10): p. 1074-80.
6. Qian, J., et al., *Caffeine consumption during early pregnancy impairs oviductal embryo transport, embryonic development and uterine receptivity in mice.* Biol Reprod, 2018. **99**(6): p. 1266-1275.
7. Klionsky, D.J., *Autophagy: from phenomenology to molecular understanding in less than a decade.* Nat Rev Mol Cell Biol, 2007. **8**(11): p. 931-7.
8. Wen, X. and D.J. Klionsky, *An overview of macroautophagy in yeast.* J Mol Biol, 2016. **428**(9 Pt A): p. 1681-99.
9. Itakura, E., et al., *Beclin 1 forms two distinct phosphatidylinositol 3-kinase complexes with mammalian Atg14 and UVRAG.* Mol Biol Cell, 2008. **19**(12): p. 5360-72.
10. Sun, Q., et al., *Identification of Barkor as a mammalian autophagy-specific factor for Beclin 1 and class III phosphatidylinositol 3-kinase.* Proc Natl Acad Sci U S A, 2008. **105**(49): p. 19211-6.
11. Song, Z.H., et al., *Germ cell-specific Atg7 knockout results in primary ovarian insufficiency in female mice.* Cell Death Dis, 2015. **6**(1): p. e1589.
12. Gawriluk, T.R., et al., *Beclin-1 deficiency in the murine ovary results in the reduction of progesterone production to promote preterm labor.* Proc Natl Acad Sci U S A, 2014. **111**(40): p. E4194-203.
13. Oestreich, A.K., et al., *The autophagy protein, FIP200 (RB1CC1) mediates progesterone responses governing uterine receptivity and decidualizationdagger.* Biol Reprod, 2020. **102**(4): p. 843-851.
14. Popli, P., et al., *Beclin-1-dependent autophagy, but not apoptosis, is critical for stem-cell-mediated endometrial programming and the establishment of pregnancy.* Dev Cell, 2023. **58**(10): p. 885-897 e4.
15. Oestreich, A.K., et al., *The Autophagy Gene Atg16L1 is Necessary for Endometrial Decidualization.* Endocrinology, 2020. **161**(1).
16. Matsunaga, K., et al., *Two Beclin 1-binding proteins, Atg14L and Rubicon, reciprocally regulate autophagy at different stages.* Nat Cell Biol, 2009. **11**(4): p. 385-96.
17. Soyal, S.M., et al., *Cre-mediated recombination in cell lineages that express the progesterone receptor.* Genesis, 2005. **41**(2): p. 58-66.
18. Zhang, Y., et al., *A transgenic FOXJ1-Cre system for gene inactivation in ciliated epithelial cells.* Am J Respir Cell Mol Biol, 2007. **36**(5): p. 515-9.
19. Chadchan, S.B., et al., *Antibiotic therapy with metronidazole reduces endometriosis disease progression in mice: a potential role for gut microbiota.* Hum Reprod, 2019. **34**(6): p. 1106-1116.
20. Kommagani, R., et al., *The Promyelocytic Leukemia Zinc Finger Transcription Factor Is Critical for Human Endometrial Stromal Cell Decidualization.* PLoS Genet, 2016. **12**(4): p. e1005937.

619 21. Teng, J.F., et al., *Polyphyllin VI Induces Caspase-1-Mediated Pyroptosis via the Induction of*
620 *ROS/NF-kappaB/NLRP3/GSDMD Signal Axis in Non-Small Cell Lung Cancer.* Cancers (Basel),
621 2020. **12**(1).
622 22. Tong, W. and J.W. Pollard, *Progesterone inhibits estrogen-induced cyclin D1 and cdk4 nuclear*
623 *translocation, cyclin E- and cyclin A-cdk2 kinase activation, and cell proliferation in uterine*
624 *epithelial cells in mice.* Mol Cell Biol, 1999. **19**(3): p. 2251-64.
625 23. Ito, S., Y. Yamamoto, and K. Kimura, *Analysis of ciliogenesis process in the bovine oviduct*
626 *based on immunohistochemical classification.* Mol Biol Rep, 2020. **47**(2): p. 1003-1012.
627 24. Liu, Q., et al., *The role of mitochondria in NLRP3 inflammasome activation.* Mol Immunol,
628 2018. **103**: p. 115-124.
629 25. Shi, Y., et al., *Echinacoside Induces Mitochondria-Mediated Pyroptosis through Raf/MEK/ERK*
630 *Signaling in Non-Small Cell Lung Cancer Cells.* J Immunol Res, 2022. **2022**: p. 3351268.
631 26. Wang, Y., et al., *Mitochondrial ROS promote macrophage pyroptosis by inducing GSDMD*
632 *oxidation.* J Mol Cell Biol, 2019. **11**(12): p. 1069-1082.
633 27. Popli, P., A.J. Sun, and R. Kommagani, *The Multifaceted Role of Autophagy in Endometrium*
634 *Homeostasis and Disease.* Reprod Sci, 2022. **29**(4): p. 1054-1067.
635 28. Choi, J., et al., *Differential induction of autophagy by mTOR is associated with abnormal*
636 *apoptosis in ovarian endometriotic cysts.* Mol Hum Reprod, 2014. **20**(4): p. 309-17.
637 29. Zhou, S., et al., *Author Correction: Menopause-induced uterine epithelium atrophy results*
638 *from arachidonic acid/prostaglandin E2 axis inhibition-mediated autophagic cell death.* Sci
639 Rep, 2020. **10**(1): p. 6915.
640 30. Fan, W., A. Nassiri, and Q. Zhong, *Autophagosome targeting and membrane curvature*
641 *sensing by Barkor/Atg14(L).* Proc Natl Acad Sci U S A, 2011. **108**(19): p. 7769-74.
642 31. Diao, J., et al., *ATG14 promotes membrane tethering and fusion of autophagosomes to*
643 *endolysosomes.* Nature, 2015. **520**(7548): p. 563-6.
644 32. Ma, X., et al., *LPS Mediates Bovine Endometrial Epithelial Cell Pyroptosis Directly Through*
645 *Both NLRP3 Classical and Non-Classical Inflammasome Pathways.* Front Immunol, 2021. **12**:
646 p. 676088.
647 33. Cookson, B.T. and M.A. Brennan, *Pro-inflammatory programmed cell death.* Trends
648 Microbiol, 2001. **9**(3): p. 113-4.
649 34. Jorgensen, I. and E.A. Miao, *Pyroptotic cell death defends against intracellular pathogens.*
650 Immunol Rev, 2015. **265**(1): p. 130-42.
651 35. Liu, J., et al., *Autophagy blockage promotes the pyroptosis of ox-LDL-treated macrophages*
652 *by modulating the p62/Nrf2/ARE axis.* J Physiol Biochem, 2021. **77**(3): p. 419-429.
653 36. Lu, Q., et al., *Homeostatic Control of Innate Lung Inflammation by Vici Syndrome Gene Epg5*
654 *and Additional Autophagy Genes Promotes Influenza Pathogenesis.* Cell Host Microbe, 2016.
655 **19**(1): p. 102-13.
656 37. Netea-Maier, R.T., et al., *Modulation of inflammation by autophagy: Consequences for*
657 *human disease.* Autophagy, 2016. **12**(2): p. 245-60.

658

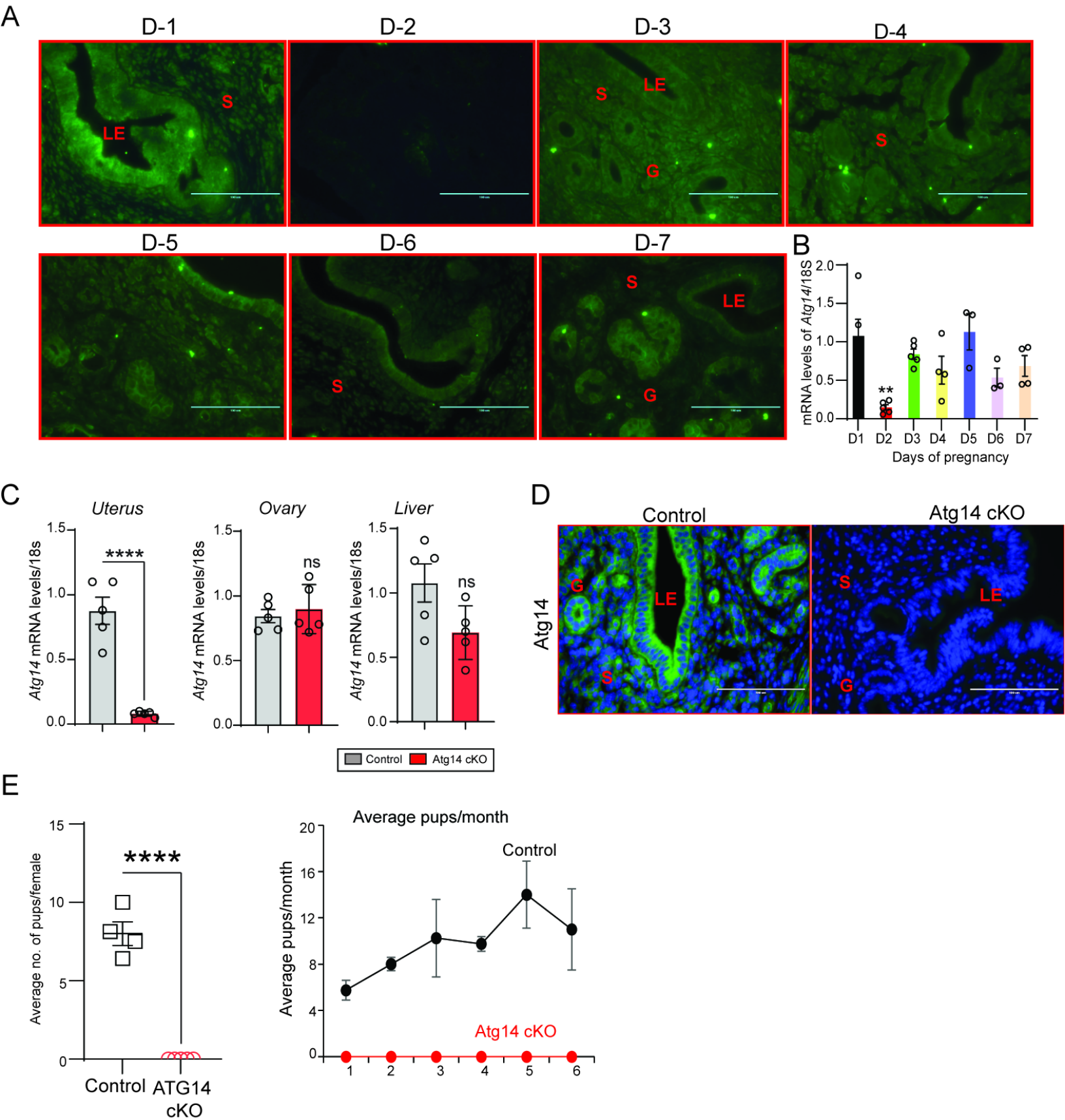
A
D-1
D-2
D-3
D-4
D-5
D-6
D-7
S
LE
G
B
mRNA levels of Atg14/18S
2.0
1.5
1.0
0.5
0.0
**
D1
D2
D3
D4
D5
D6
D7
Days of pregnancy
C
Uterus
Ovary
Liver
Atg14 mRNA levels/18s
****
ns
Control
Atg14 cKO
D
Control
Atg14 cKO
Atg14
E
Average no. of pups/female
15
10
5
0
****
Control
ATG14 cKO
Average pups/month
Average pups/month
20
16
12
8
4
0
Control
Atg14 cKO
1
2
3
4
5
6

Figure 1

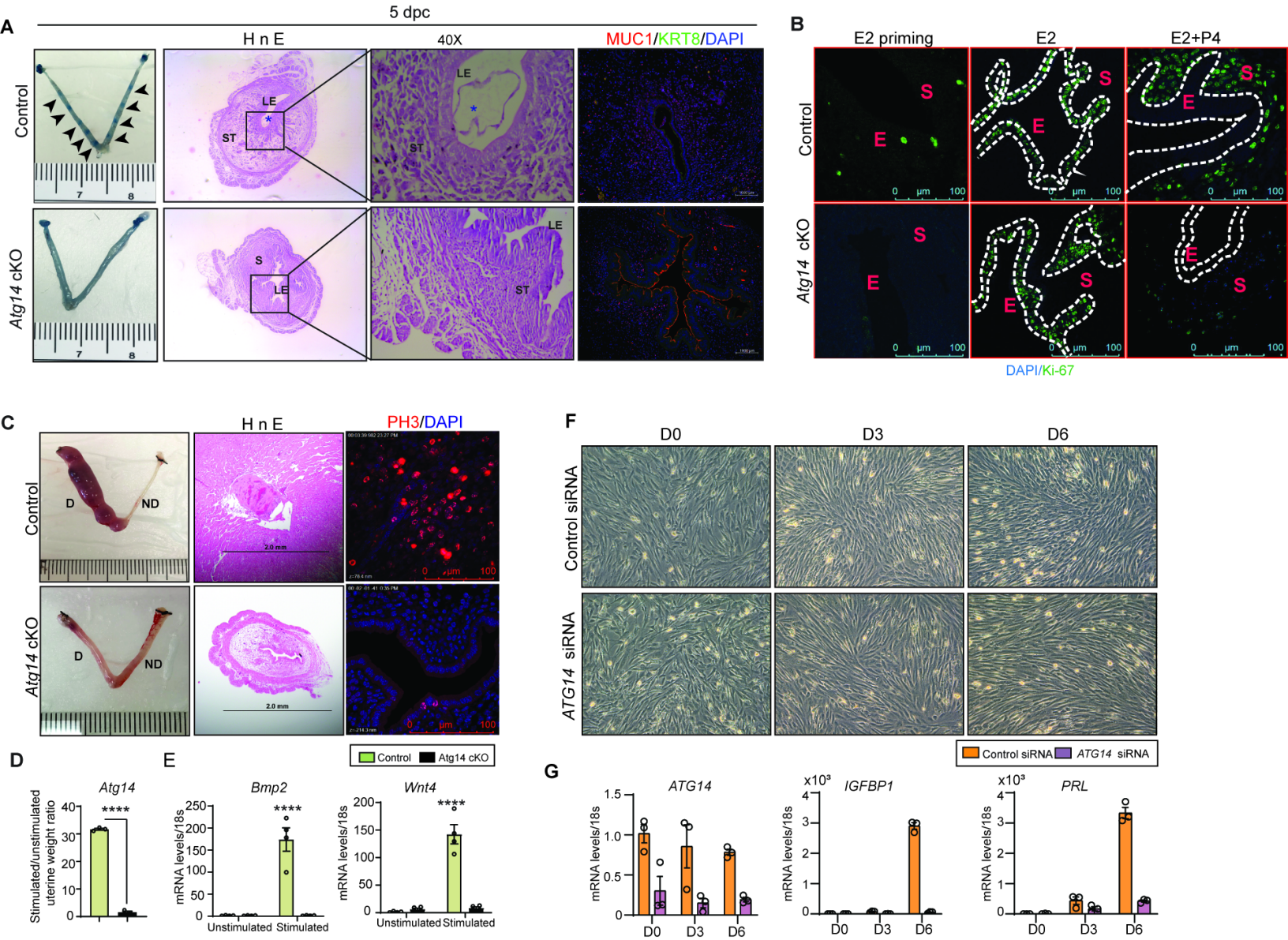
A
5 dpc
H n E
40X
MUC1/KRT8/DAPI
Control
Atg14 cKO
LE
ST
S
B
E2 priming
E2
E2+P4
Control
Atg14 cKO
S
E
0 µm 100
DAPI/Ki-67
C
H n E
PH3/DAPI
Control
Atg14 cKO
D
ND
2.0 mm
F
D0
D3
D6
Control siRNA
ATG14 siRNA
D
Atg14
Stimulated/unstimulated uterine weight ratio
****
E
Control
Atg14 cKO
Bmp2
Wnt4
mRNA levels/18s
Unstimulated
Stimulated
G
Control siRNA
ATG14 siRNA
ATG14
IGFBP1
PRL
x10³

Figure 2

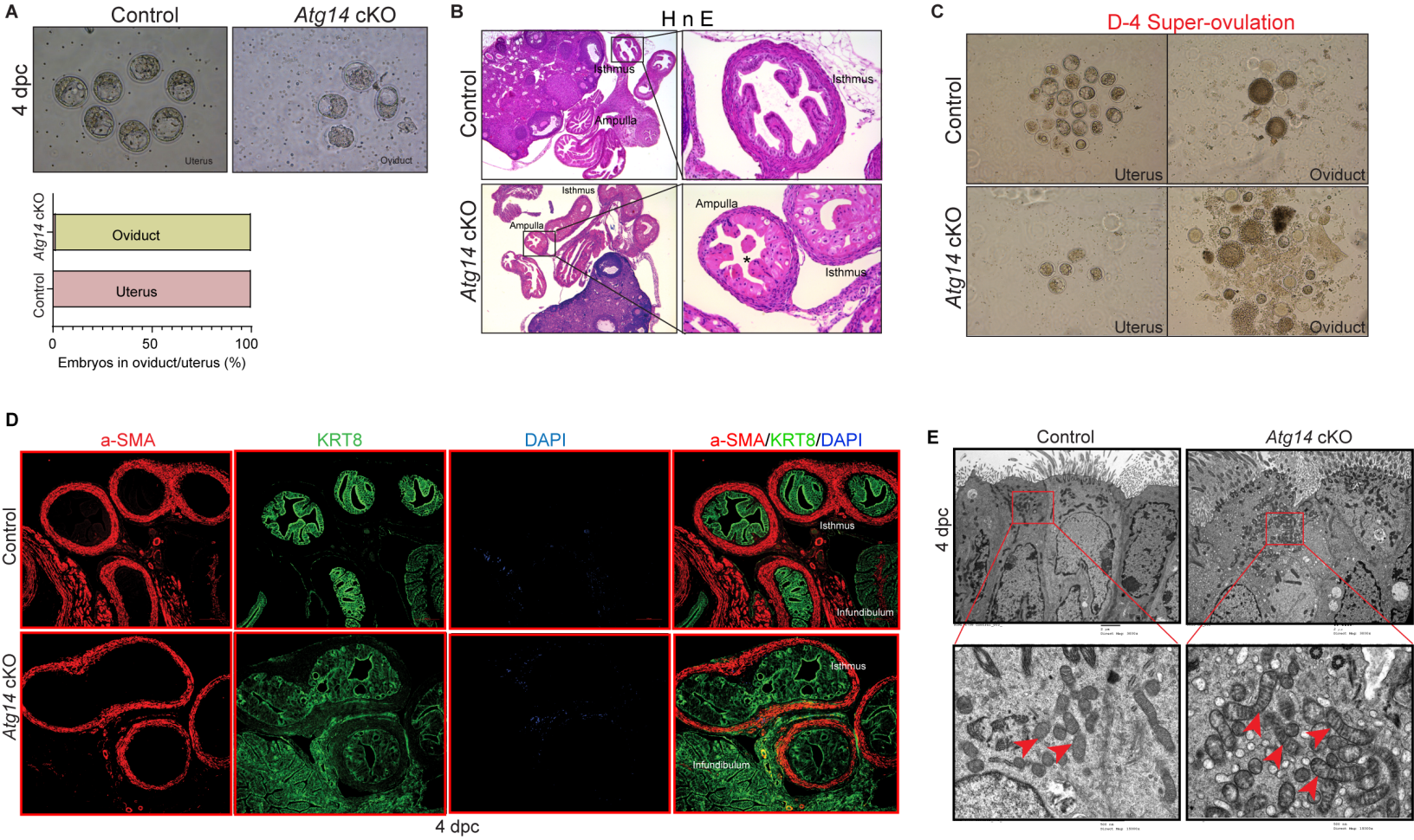
A
Control
Atg14 cKO
4 dpc
Uterus
Oviduct
Atg14 cKO
Control
Oviduct
Uterus
0
50
100
Embryos in oviduct/uterus (%)
B
H n E
Control
Atg14 cKO
Isthmus
Ampulla
Isthmus
Ampulla
Isthmus
C
D-4 Super-ovulation
Control
Atg14 cKO
Uterus
Oviduct
Uterus
Oviduct
D
a-SMA
KRT8
DAPI
a-SMA/KRT8/DAPI
Control
Atg14 cKO
Isthmus
Infundibulum
Isthmus
Infundibulum
4 dpc
E
Control
Atg14 cKO
4 dpc

Figure 3

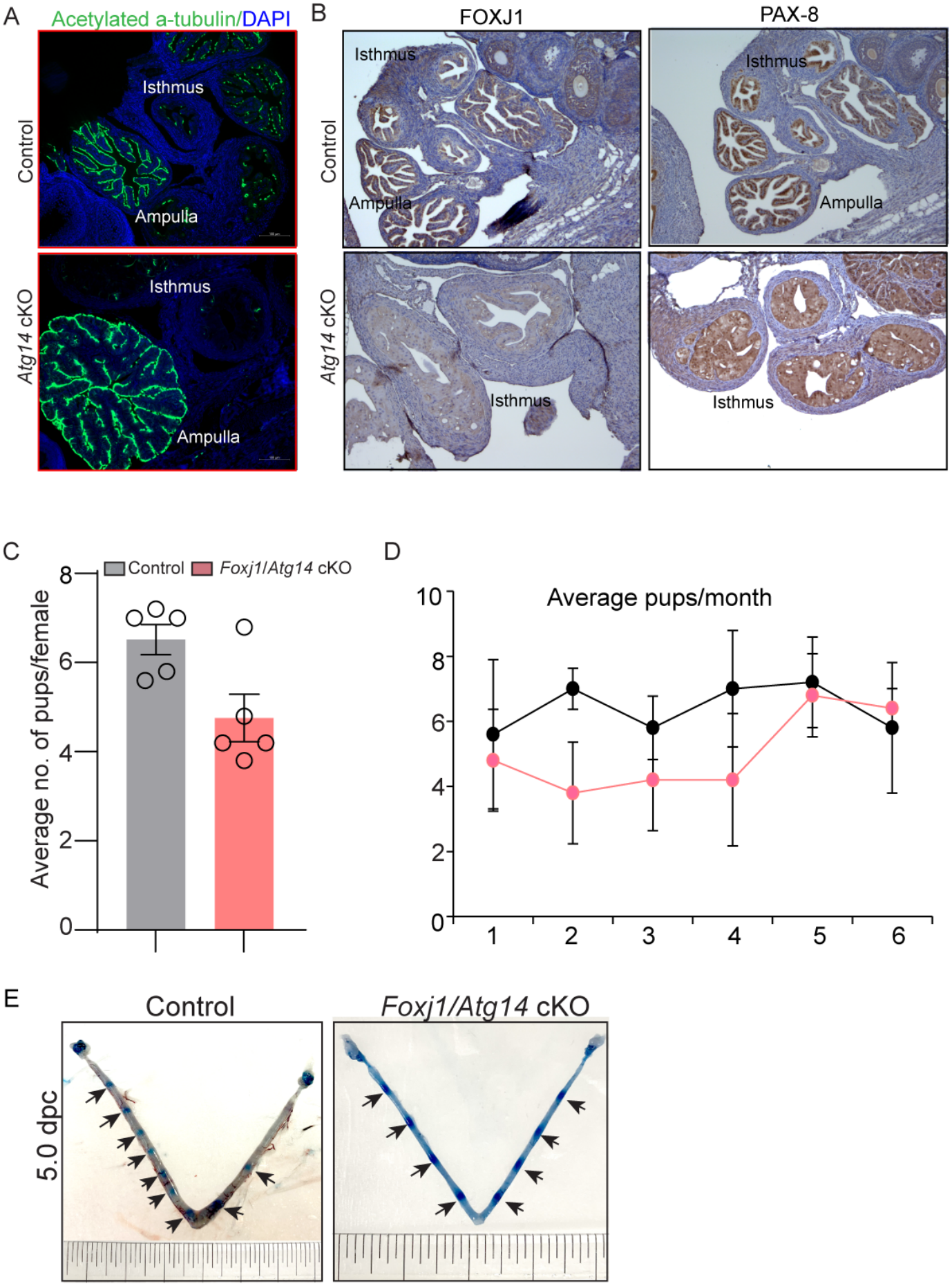
A
Acetylated a-tubulin/DAPI
Control
Isthmus
Ampulla
Atg14 cKO
Isthmus
Ampulla
B
FOXJ1
PAX-8
Control
Isthmus
Ampulla
Isthmus
Ampulla
Atg14 cKO
Isthmus
Isthmus
C
Control
Foxj1/Atg14 cKO
Average no. of pups/female
0
2
4
6
8
D
Average pups/month
0
2
4
6
8
10
1
2
3
4
5
6
E
Control
Foxj1/Atg14 cKO
5.0 dpc

Figure 4

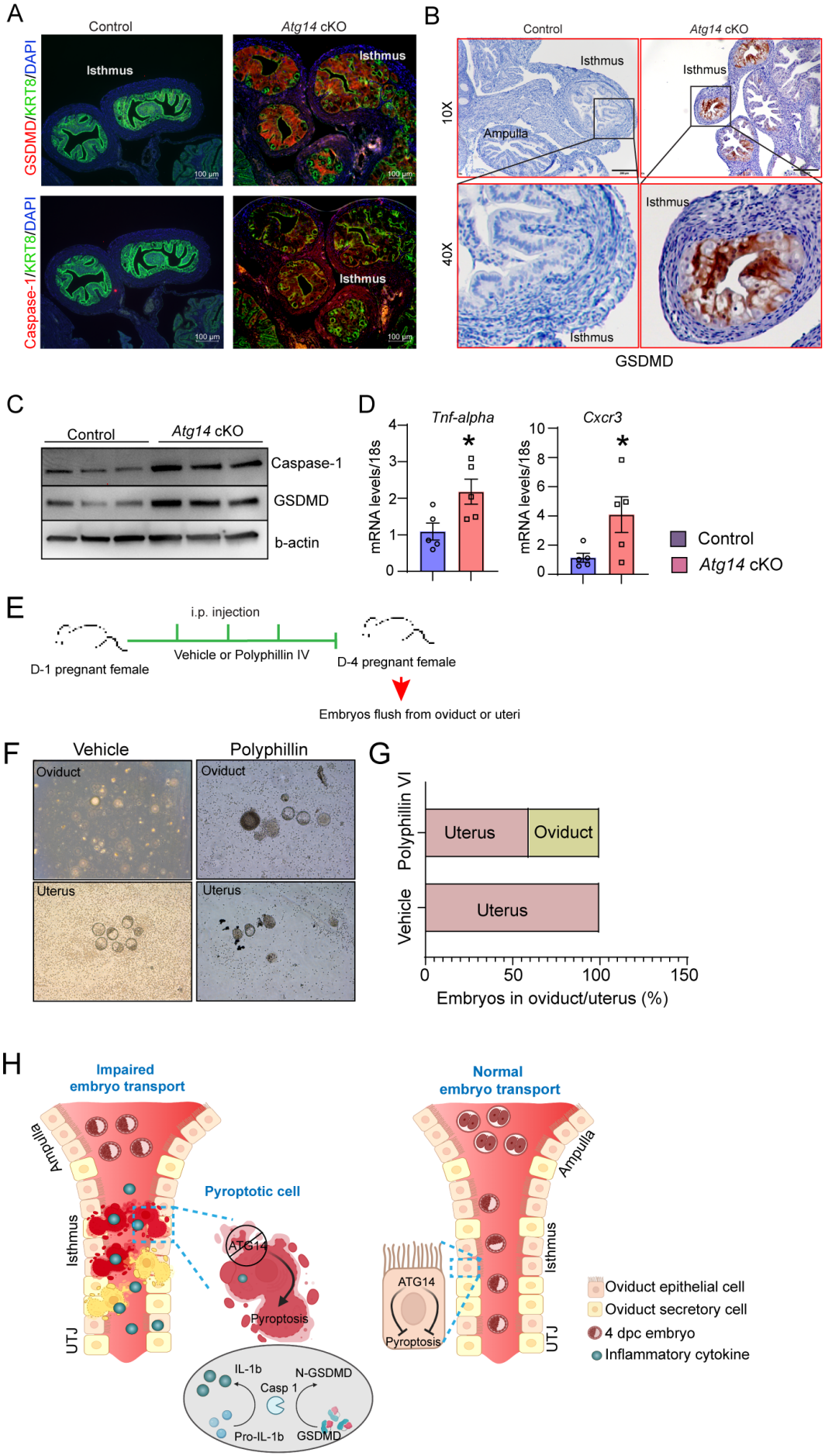
A
Control
Atg14 cKO
GSDMD/KRT8/DAPI
Caspase-1/KRT8/DAPI
Isthmus
100 μm
B
Control
Atg14 cKO
10X
40X
Isthmus
Ampulla
GSDMD
C
Control
Atg14 cKO
Caspase-1
GSDMD
b-actin
D
Tnf-alpha
Cxcr3
mRNA levels/18s
Control
Atg14 cKO
E
i.p. injection
Vehicle or Polyphillin IV
D-1 pregnant female
D-4 pregnant female
Embryos flush from oviduct or uteri
F
Vehicle
Polyphillin
Oviduct
Uterus
G
Polyphillin VI
Vehicle
Uterus
Oviduct
Embryos in oviduct/uterus (%)
H
Impaired embryo transport
Normal embryo transport
Ampulla
Isthmus
UTJ
Pyroptotic cell
ATG14
Pyroptosis
IL-1b
N-GSDMD
Casp 1
Pro-IL-1b
GSDMD
Oviduct epithelial cell
Oviduct secretory cell
4 dpc embryo
Inflammatory cytokine

Figure 5